Microstructural modeling of the mechanical behavior of open-cell polyurethane foams

Fioole, J.C.J.

Award date:
2011

J.C.J. Fioole
december 2011

Microstructural modeling of the mechanical behavior of open-cell polyurethane foams.

J.C.J. Fioole
Report number mt 12.06

Supervisors:
Dr. Ir. J.G.F. Wismans
Dr. Ir. J.A.W. van Dommelen
Prof. Dr. Ir. M.G.D. Geers

Eindhoven University of Technology
Department of Mechanical Engineering
Mechanics of Materials

December 22, 2011

1 Summary

Cellular solids, also called foams, are a special class of materials. They can be divided into two classes: natural cellular solids and man made cellular solids. Natural cellular solids are bone and wood. Man made cellular solids can be made from all kinds of materials, ranging from ceramics to polymers. The excellent specific strength, light weight and energy absorption are unique. These properties are directly correlated to the micro-structure and base material of the foam.

In order to investigate the important foam properties X-ray computed tomography is used, as a non-destructive method, to obtain 3D images of the foam. An image analysis is carried out to extract statistics about the foam's morphology. Including strut length distribution, strut thickness, cell shape and orientation.

These statistical foam properties are used as an input to create a periodic 3D foam model. Using a periodic Voronoi tessellation as a template for the foam model. A regular isotropic Kelvin cell is used as starting point for increasingly less regular foam structures.

Finite element simulations are performed on the foam models and the mechanical response is compared with a reference experiment and simulations. The macroscopic mechanical response is explained by the investigating the micro-structure of the foam models. Also the volumetric response of the foam models are investigated in compression and tension.

Contents

2 Introduction

Everybody encounters cellular solids on a daily basis, while doing the dishes using a sponge or eating bread, see figure 1(a). Also bones, in human and animal bodies, and many packaging materials used for protection are cellular solids. These cellular solids consist of an interconnected network of solid struts or plates which form the micro-structure of the material. 3D cellular solids are called foams, and when the micro-structure consists of by struts and the faces of the cell are open, they are called open-cell foams, as depicted in figure 1(b). Here the individual struts, which build up a cell, are clearly visible. On the other hand, when the faces of the cells of the foam are solid, it is referred to as a closed-cell foam, see figure 1(c). There are also 2D cellular solids like honeycombs. These are often used in sandwich panels to reinforce the panels without adding much weight, as shown in figure 1(d).

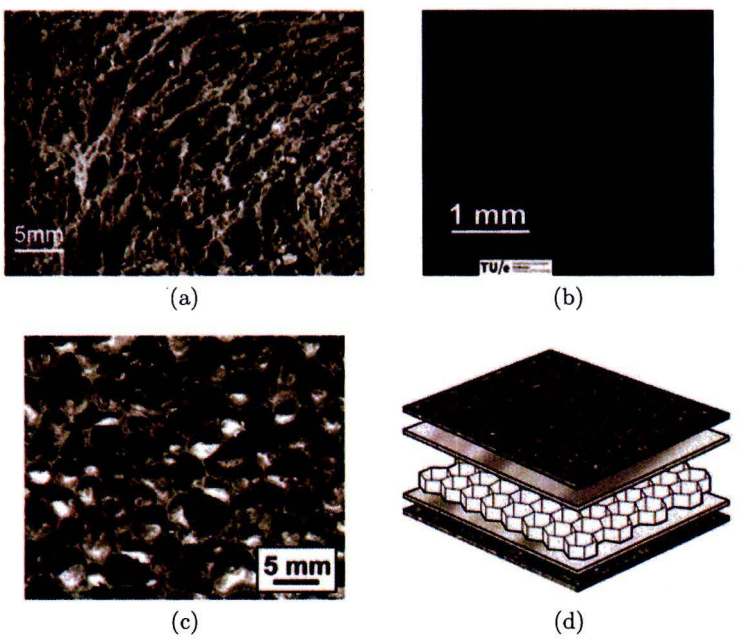

(a) (b) (c) (d)

Figure 1: The micro-structure of four cellular solids: micro-structure of bread Z. Liu and M.G. Scanlon [1] (a), an open-cell polyurethane sponge (b), an aluminium closed-cell foam (from en.wikipedia.org) (c) and a 2D honeycomb used in a sandwich panel (from www.nauticexpo.com) (d).

2.1 Foam properties

Because foams are light weight, have an excellent specific strength and good energy absorption properties, they are used in many applications such as insulation, packaging and structural use. The high energy absorption is one of the remarkable properties of foam and is one of the reasons why foams are used as packaging materials. The manner in which a foam absorbs energy is best explained considering the stress-strain response of a foam.

When a compressive load is applied to a foam, see figure 2(a), the response will first be elastic (1), followed by a plateau stress (2) and finally densification (3). For an open-cell foam, the elastic region is controlled by elastic bending of the struts until the struts start to buckle. When this happens, the plateau stress is reached and the stress remains the same until the cells collapse and contact between the struts occurs. Then the densification region starts and the stress increases rapidly.

The energy that is stored and absorbed by the foam is equal to the area under the stress-strain curve, as depicted gray in figure 2(b). The large energy absorbtion and plateau stress makes foam good packaging materials. A product is safely protected by foam during impact when the plateau stress of the foam is lower then the maximum allowable stress and the foam can absorb enough energy before densification occurs.

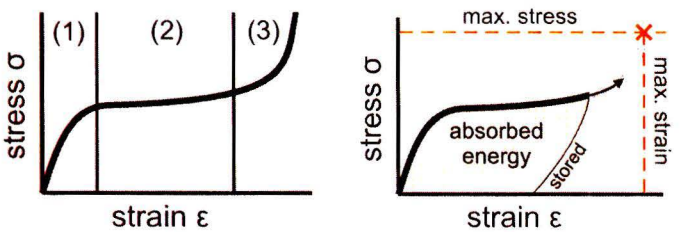

(a) (b)

Figure 2: The stress-strain response of a foam (a), where (1) is the elastic region, (2) the plateau stress and (3) the densification. The energy that is stored and absorbed by the foam is shown by the grey area in (b).

The mechanical properties of a foam originate from a combination of the micro-structure and the foam base material. An important structural characteristic is the relative density of the foam ϕ which is described by:

$$\phi = \frac{\rho^*}{\rho_s} \tag{1}$$

where ρ^* is the density of the foam and ρ_s is the density of the base material. Foams have relative densities which are less than about 0.3, with most foams having a relative density which is even smaller, as low as 0.003. The relative density can be used as a scaling parameter to predict the Young's modulus of a foam E^*, which is described for open-cell foams according to Gibson and Ashby [2] by:

$$\frac{E^*}{E_s} \approx \phi^2 \tag{2}$$

where E_s is the Young's modulus of the base material.

2.2 Previous studies

Numerous studies are performed on the subject of foams. An elaborate overview of many aspects of cellular solids is presented by Gibson and Ashby [2]. In this work, for different types of foam, aspects ranging from the micro-structure to the fabrication of foams are discussed.

Dillard et al. [3] presented an experimental study on the compressive and tensile behavior of open-cell nickel foams. The nickel foam was fabricated via cathodic magnetron nickel sputtering of a polyurethane foam template. 3D images of the nickel foam were made using X-ray computed tomography (X-ray CT). These images were analyzed in order to obtain the foam morphology. After compression and tensile tests the morphology of the nickel foam were again analyzed in order to see the influence of compression and tension on the micro-structure of the nickel foam. The geometrical anisotropy of the micro-structure was shown to be related to the anisotropic elastic response of the nickel foams.

An analytical study of the elastic response of Kelvin cells was made by Zhu et al. [4]. The Kelvin cell was proposed by Lord Kelvin [10] and almost minimizes surface area, which indicates that it is a good representative cell for open-cell foams. The elastic properties were calculated by considering the bending, twisting and extension of the struts and showed that all of these deformation mechanisms are important in order to determine the elastic moduli. The foam bulk modulus was predicted to vary linearly with the relative density of the considered foam, which means that the Poisson's ratio approaches 0.5 for low density foams. By calculating the anisotropy factor of the Kelvin cell it was shown that a Kelvin cell is elastically almost isotropic.

In the work of Takahashi et al. [5], a Kelvin cell was used to represent aluminium foam. The Kelvin cell was modelled with 3D finite elements, and

a comparison is made between a geometry with uniform strut cross section and a geometry where the cross section increases in thickness along the length of the struts. In their work, a plastic material model was used and it was shown that both the plastic material model and the non-uniformity of the strut cross-sectional area along the strut length are important features for the yield and buckling behavior of the aluminium foams represented by a Kelvin cell.

Jang et al. [6] also used X-ray CT to obtain 3D images of a foam. These images where used to study the morphology of the foam, which was used to build finite element foam models. The most idealized model used was a Kelvin cell and the more realistic models were based on models created by the "Surface Evolver" [7]. It appeared that the most realistic models yielded the best results. However in view of the numerical efficiency, a Kelvin cell was recommended as a good engineering tool for calculating the elastic properties of foams.

In the work of Wismans [8] a study was performed on an open-cell polymeric foam. X-ray CT was used to obtain a 3D image of the foam's micro-structure and a finite element model of the foam was directly made from the 3D image of the foam. The foam model used in the finite element simulations is thus a very precise representation of the micro-structure of the examined foam. In addition to a realistic micro-structure, a material model called the "Eindhoven Glassy Polymer" (EGP) model [9] was used to properly describe the intrinsic material behavior. The EGP model is a visco-plastic material model. It was shown that the visco-plastic behavior is important to describe the buckling of struts. One of the main conclusions was that both the intrinsic material behavior as well as the micro-structure of the foam have a great influence on the response of a polymeric foam.

2.3 Problem statement and outline

As was shown by previous studies, it is important to model both the micro-structure and intrinsic material behavior, when performing finite element simulations on foams. However, whether the "Surface Evolver" or 3D images of the foam's micro-structure are used to create a realistic foam model, it is numerically expensive to calculate the response of realistic foam structures. In this work it is investigated how much detail of the micro-structure, when using a proper intrinsic material model, is needed to describe the response of an open-cell polymeric foam.

Therefore, the geometric characteristics of a foam are obtained using X-

ray computed tomography and image analysis techniques in chapter two. In chapter three, a periodic foam structure, based on the Kelvin cell and perturbations there of, is created using the foam geometric characteristics obtained in chapter two. In chapter four the results of increasingly more realistic foam structures are presented, starting with a periodic Kelvin cell and finishing with an anisotropic foam structure originally based on Kelvin cells. Finally, there is a discussion on the results and some recommendations are made for future research.

3 Foam morphology

In this chapter, an open-cell polyurethane (PUR) foam is examined in order to obtain statistical information about the micro-structure. The obtained properties of the foam's morphology will be used to create a periodic finite element mesh representing the examined foam, as explained in chapter 4.

3.1 X-ray Computed Tomography

In order to obtain a 3D image of a real PUR foam, X-ray Computed Tomography (CT) is used. X-ray CT is a non destructive technique to obtain the microstructure of the foam. In CT, a sample is placed on a rotation stage and rotated over 360°. The foam sample is exposed to X-rays emitted from an X-ray source and angular projections of the sample are recorded by a CCD detector, see figure 3. A 3D image, consisting of voxels, is reconstructed from all projections.

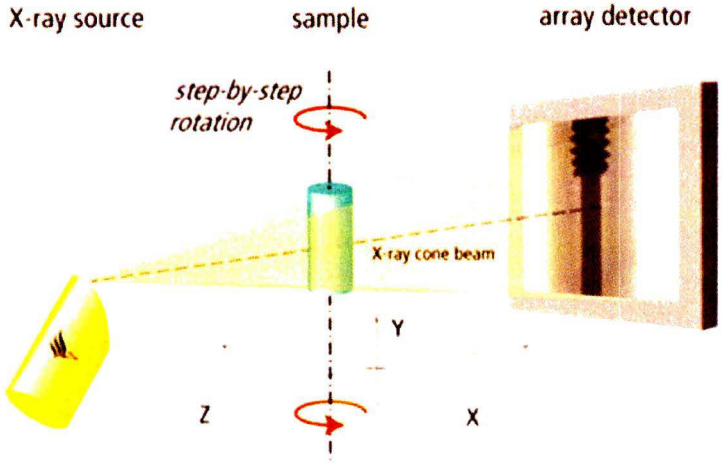

Figure 3: Schematic representation of an X-ray CT setup. (http://www.phoenix-xray.com).

The resolution, or voxel size v_s which is in this work 5 μm, of the 3D image is limited by the spot size [8] of the X-ray source and is related to the pixel size of the detector p_s and the magnification M by:

$$v_s = \frac{p_s}{M}. \tag{3}$$

The reconstructed volume consists of gray values, which can be visualized by a histogram, see figure 4. In the histogram two distinct peaks are visible. The peak which is indicated by the two vertical boundaries represents PUR and the other peak represents air. In order to obtain a binary 3D image, where a black voxel represents PUR and a white voxel represents air, the gray values has to be segmented. However there is no objective boundary between the two peaks in the histogram in order to segment the volume into air and PUR. Therefore knowledge of the specific density of the original PUR sample is used to segment the 3D image so that the obtained binary 3D image has the same specific density.

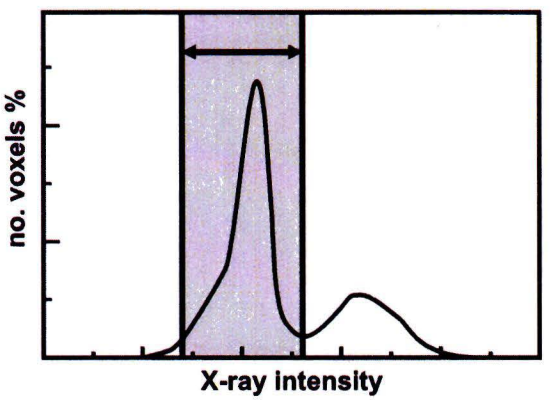

Figure 4: A schematic representation of a histogram of the voxel gray-values obtained by the X-ray CT. The vertical boundaries are used to segment the scan of the PUR foam.

3.2 Skeletonization

The binary 3D image contains all the information of the geometry of the microstructure of the foam. By applying a skeletonization algorithm, the skeleton of the microstructure is obtained. The advantages of a skeleton representation of the foam are that struts and vertices in the foam are more easily defined. The skeletonization algorithm used in this work is developed by Reniers [11].

The curve skeleton is shown in figure 5. The "Skeleton Sandbox", the code of Reniers, can handle 3D images with a maximum of 300^3 voxels. Therefore the binary 3D image with a size of 500^3 is divided in eight overlapping parts of 300^3 voxels. Each 3D image thus has an overlap of 100 voxels with its

neighbors. This overlap is necessary because the curve skeleton is not well defined at the faces of the 3D images. In figure 5, it can be observed that in the right top corner the skeleton is not computed at all and in figure 6(a) the skeleton at the boundary of the domain is computed wrongly. Therefore, the skeletons are overlapped, cropped by 50 voxels at the boundary faces and finally combined, see figure 6(b).

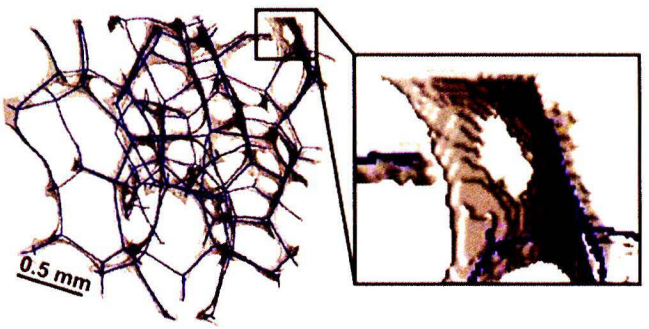

Figure 5: The 3D image representing the PUR foam and the computed curve skeleton. The skeleton is computed incorrectly in the top right corner of the foam volume.

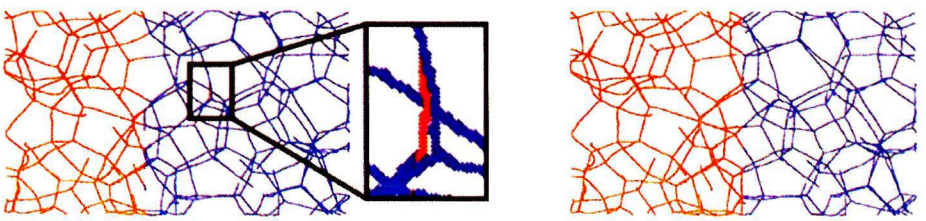

(a) (b)

Figure 6: Two neighboring skeletons are overlapped. The red skeleton is computed incorrectly near the boundary(a), both skeletons are cropped and combined (b)

3.3 Vertices and struts

A vertex is junction of struts. Most vertices are junctions of four struts meeting at a mean angle of 109° [3]. The vertices contain a significant concentration of material. A common vertex is depicted in figure 7(a). The four struts meet at angles of around 109°. The edges of the triangular struts join smoothly. In figure 7(b), two vertices are depicted which are connected by a short thick strut. When this strut would have been a bit shorter, the two vertices would join into a single vertex with 6 struts. A solid face is depicted in figure 7(c), although it is a matter of definition whether this should be called a solid face or a vertex with 8 struts joining (one strut is not visible in the figure).

Now that the skeleton is computed the struts and vertices have to be identified. A path following algorithm is written which follows the skeleton until a vertex is found. From this vertex, the path following algorithm continues until all vertices and struts are identified. The positions and connectivity of all vertices are now known.

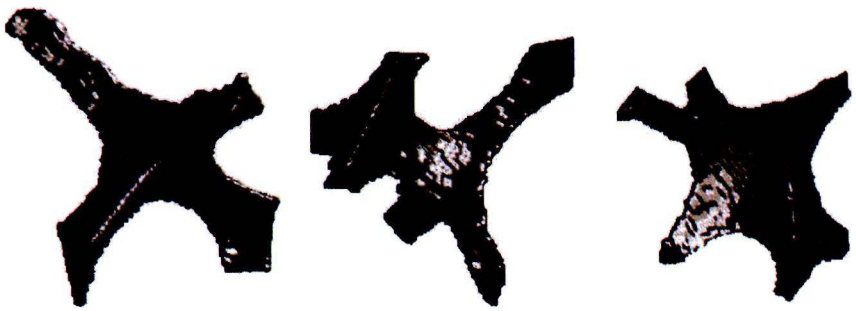

(a) (b) (c)

Figure 7: A common vertex with four struts (a), two vertices close to each other connected with a short thick strut (b) and a closed face (c).

All struts are defined as straight lines between vertices. The strut lengths are defined as the distance between the connected vertices. The distribution of strut lengths is examined in three volumes of the foam: two volumes of $2.5^3\,\mathrm{mm}^3$ and one volume of $1.5^3\,\mathrm{mm}^3$ and is depicted in figure 8.

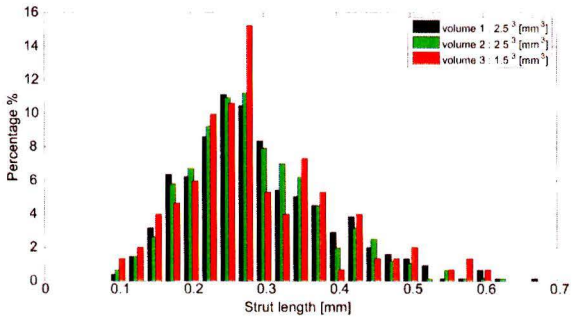

Figure 8: Strut length distribution found in the PUR foam.

3.4 Strut thickness

In order to obtain the strut thickness, a third order polynomial is fitted through the voxels of the skeleton of a single strut. Cross-sections of the strut are made perpendicular to the fitted curve. All voxels which represent PUR are detected in these slices and the shape and size of the cross-section are determined, see figure 9. The red dots represent the skeleton voxels, the green curve is fitted through these voxels and the slices are visualized, with the black voxels representing the cross section of the strut.

The cross sectional area of the struts is triangular with a slight curvature of the edges forming a three cusp hypocycloid know as Plateau border [12]. The Plateau border is not quite visible in the center of the struts due to an insufficient resolution of the 3D images. Near the vertices, the Plateau border is visible because the strut increases in thickness.

When determining the cross-section of the struts, a problem arises near the vertices. The struts are not well defined near the vertices. As depicted at the left in figure 10, a cross section is obtained through material that clearly belongs to a neighboring strut. Because the struts are not well defined at the vertices, the cross sections near the vertices are not taken into account later on.

The areas of the cross sections are plotted along the normalized length of the struts in figure 11(a). The color of the lines indicates the length of the strut. Long struts have a smaller cross sectional area than the shorter struts and have a more uniform cross section in the middle of the struts, as can be clearly seen in figure 11(b) where the struts are sorted depending on their lengths.

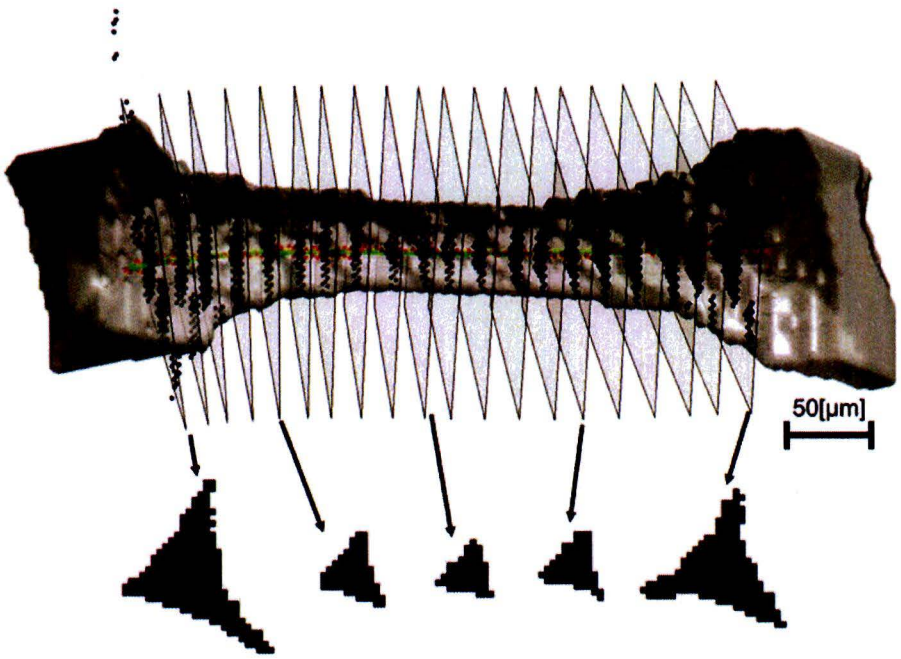

Figure 9: Cross-sections of a strut of the segmented data.

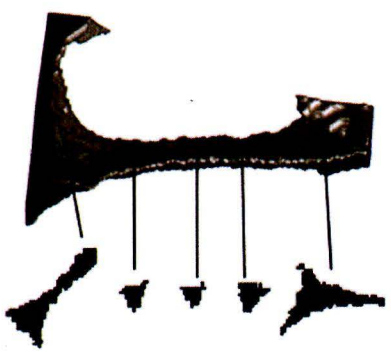

Figure 10: Cross sections derived near or at the vertices can contain material that clearly belongs to a neighboring strut.

In figure 12, the area in the middle of the struts is plotted against the strut length. A clear trend is observed, with shorter struts being thicker than longer struts in the middle region of the struts. The information of the cross section in the middle of the struts is rather reliable because the struts are well defined here and no extra area that belongs to the vertices or other struts is taken into account. A third order curve is fitted through the data ranging from strut length 0.1 mm to 0.4 mm. There are too few data points for struts longer then 0.4 mm to fit the data, so the same mid area is assumed for struts longer than 0.4 mm as for struts that are 0.4 mm, visualized by the dotted line.

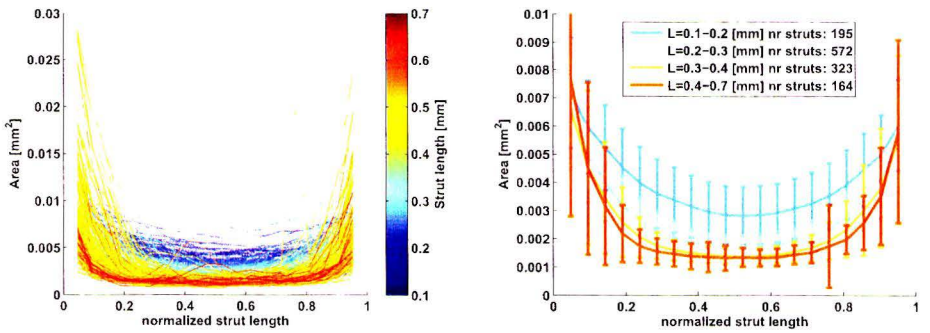

(a) (b)

Figure 11: Cross section of the struts plotted versus the normalized length of the struts.

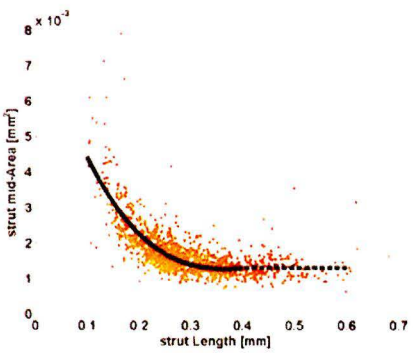

Figure 12: Area in the middle of the struts plotted versus the length of the struts. The black line represents a third order fit.

3.5 Cell segmentation

In order to determine the cell sizes and shapes, separate cells are identified. To segment the connected air bubbles in the open-cell PUR foam, watershed segmentation is used [13]. A 2D example, in which a binary image of two overlapping circles has to be segmented is depicted in figure 13. First, a distance transform is applied to the binary image, where every black pixel is assigned a value that represents the Euclidean distance to the nearest white pixel. This distance transform is represented with a height-plot, in figure 13b. A local minimum is present in between the two peaks. This minimum is used to segment the image into two regions, see figure 13c.

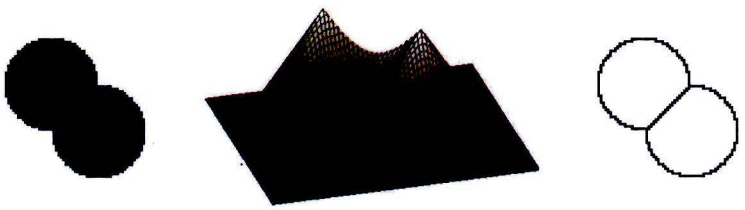

(a) (b) (c)

Figure 13: To segment the two overlapping circles (a), a distance transform is applied (b). From this distance transform, a watershed segmentation is calculated (c).

However, watershed segmentation usually results in over-segmentation due to imperfections in the image, as illustrated in figure 14a. Here, more local minima are found and thus the watershed segmentation results in more segmented areas, see figure 14b.

Watershed segmentation is also applicable to 3D image data. In figure 15(a), a slice from voxel data containing 500^3 voxels is depicted after the 3D watershed segmentation is applied. It can be clearly seen that the cells are over-segmented. As in the 2D example with imperfect circles, imperfections are responsible for the over-segmentation. However, the imperfections at the boundaries of the cells are related to the resolution of the image. By lowering the resolution, the imperfections change and thus the manner in which the cells are over-segmented changes as well. In figure 15b the resolution of the voxel shape is reduced from 5 μm to 15 μm resulting in a data set containing 166^3 voxels, which leads to a different segmentation. By overlaying several segmentations of different resolutions, the correct cell segmentation is ob-

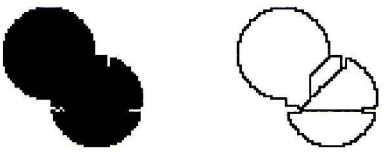

(a) (b)

Figure 14: Two overlapping circles with imperfections at the edges of the circles (a). The watershed segmentation results in an over-segmentation (b).

tained, see figure 15(c) and 15(d). Since after this procedure there are still some cells split in two, some manual adjustments are made afterwards.

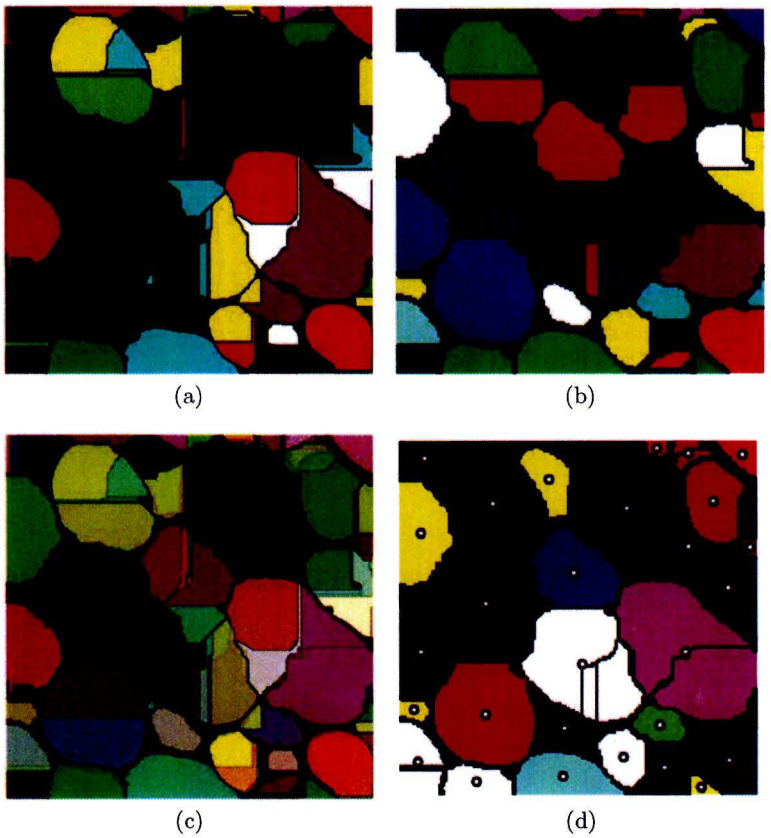

Figure 15: A slice of the watershed segmentation of the original voxel data containing 500^3 voxels (a), and a slice of the watershed segmentation of the voxel data containing 166^3 voxels. By overlaying the two segmentations (c), a better segmentation is obtained (d). However, it is still necessary to manually adjust this final segmentation afterwards.

3.6 Cell morphology

From these segmentations, the separate cells are examined. An isolated cell is depicted in figure 16(a). In order to obtain information about the orientation of the cell and the roundness, an ellipsoid is fitted, using a least squares ellipsoid fitting [14]. In order to obtain a point cloud through which the ellipsoid is fitted, the convex hull of the segmented cell is calculated, see figure

16(b). The points which lie on the convex hull are used as a point cloud for the ellipsoid fitting, see figure 16(c). The ellipsoid has some cropped faces, because it is plotted in the same domain as the original segmented cell. Also the major-axis and the two minor-axes are plotted with a magnification of 1.2 for better visualization.

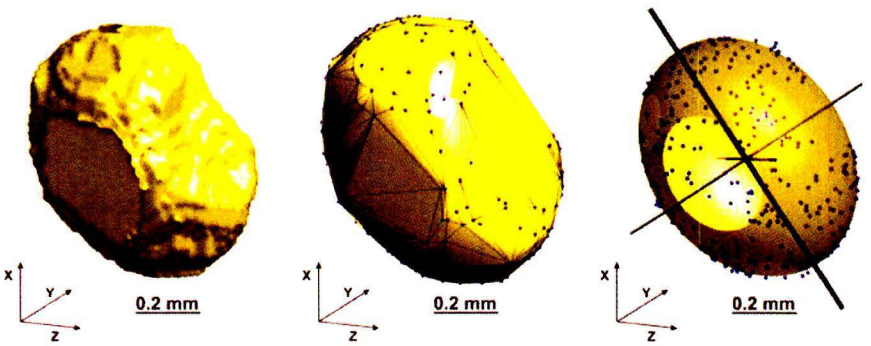

(a) (b) (c)

Figure 16: A segmented cell (a), the convex hull of the cell is computed in order to obtain a point cloud depicted by the blue points (b). A least square ellipsoid fitting is performed through the point cloud representing the isolated cell (c). The major-axis and the two minor-axes of the ellipsoid are depicted with a small elongation.

In total, 45 complete cells from a foam volume of $2.5^3\,\mathrm{mm}^3$ are examined. Incomplete cells located at the boundary and badly segmented cells are excluded from the analysis. The cells have a mean volume of $0.14\,\mathrm{mm}^3$ and the volume distribution is depicted in figure 17(a). Most cells have a volume of around $0.14\,\mathrm{mm}^3$ with a few larger cells. It must be stated that it is possible that the considered volume might be a bit small in order to be representative. It might be possible that the examined foam has a wider distribution of cell sizes but that there are not enough complete larger cells in the considered volume of foam to be analyzed.

The fitted ellipsoid is used to extract the general shape and orientations of the cells. The ellipsoid-ratio is defined as the length of the major-axis divided by the mean lengths of the two minor-axes, which have more or less the same length for all cells. A larger ellipsoid-ratio means a more elongated ellipsoid. For example, a sphere has a ratio of 1. The distribution of ellipsoid-ratio is depicted in figure 17(b). The mean value of the ellipsoid-ratio is 1.34. The

orientation of a single cell is defined as the orientation of the major-axis of the fitted ellipsoid. The orientations of the 45 segmented cells are depicted in an equal area pole figure in figure 17(c). Here the X-projection is depicted and a clear orientation is present in the X-direction.

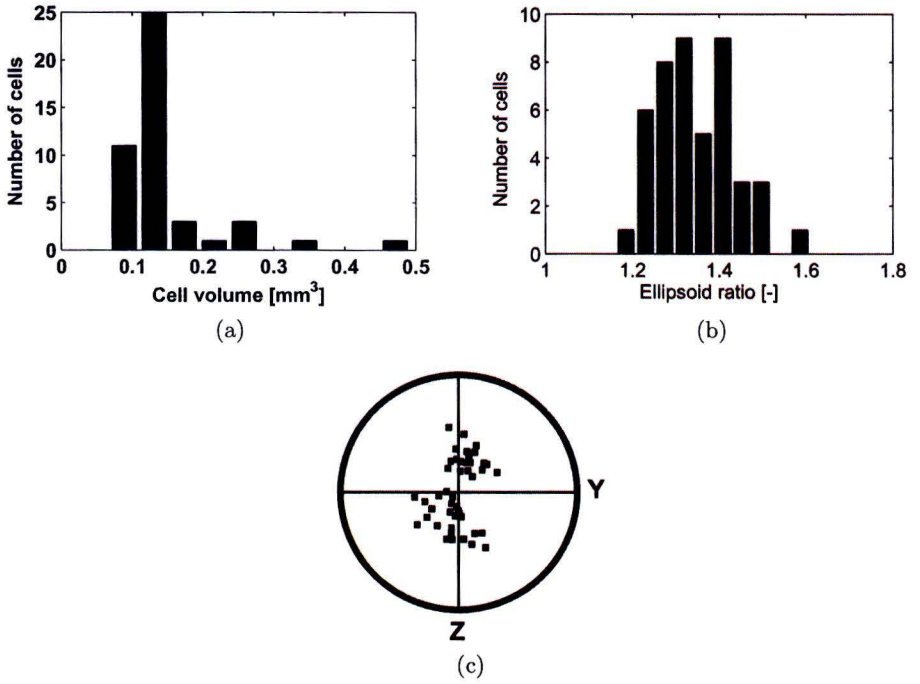

Figure 17: The properties of 45 complete cells. The cell volumes, with a mean volume of $0.14\,\mathrm{mm}^3$, are plotted in a histogram (a), the ratio between the major-axis and the minor-axes of the ellipsoids (b) and the orientation of the major-axis of the ellipsoids are depicted in an equal area pole figure (c).

Other morphological properties of the cells are the number of faces per cell and the number of struts per face. In order to investigate these properties, the PUR material surrounding the cells is isolated, see figure 18(a). More precise, the vertices surrounding a single cell are isolated. This is done by calculating the 3D euclidian distance transform of an isolated cell. Using the distance transform of the segmented cell, all vertices surrounding the cell which lay within a preset distance perpendicular to the surface of the cell can

be identified, see figure 18(b). Here the black volume is the preset distance perpendicular to the surface of the cell. All vertices which lie within this volume form a cell together.

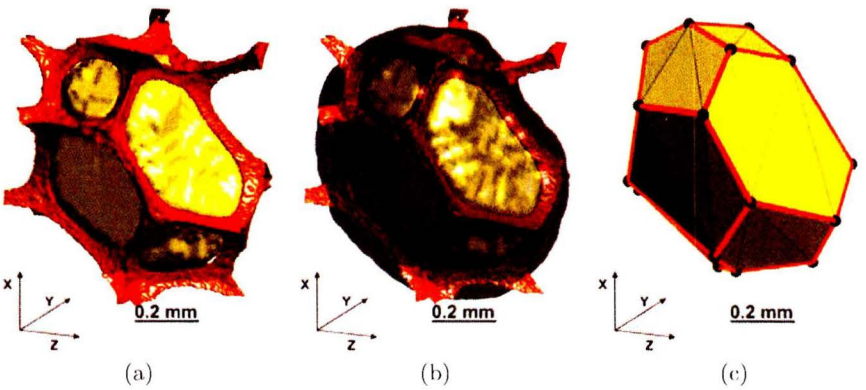

(a) (b) (c)

Figure 18: An isolated cell with the surrounding foam structure (a), the black volume which should contain all vertices which form the isolated cell (b) and the identified vertices in black and struts in red which build up the isolated cell (c).

Now that the corresponding vertices of the isolated cell are identified, as depicted by black dots in figure 18(c), the faces of the cell are reconstructed. The convex hull defined by the vertices is computed, which is a representation of the general shape of the cell in triangles depicted with the black lines. The outward facing face-normals of these triangles are computed. The triangles which have similar orientated face-normals are defined as one face. The corresponding vertices of a single face are connected by struts surrounding the perimeter of the face. The distribution of faces per cell is depicted in figure 19(a) and the distribution of struts per face is depicted in figure 19(b). The mean number of faces per cell is found to be 12.9 and the mean number of struts per face is found to be 5.25. These results are in good correspondence to the work of Dillard et al. [3] where a nickel foam was analyzed. The analyzed nickel foam was created using a PUR foam template. The mean number of faces per cell which Dillard et al. found was 13.02 and the mean number of struts per face was 5.07.

One face is build up by 8 struts. However after examining this face, it can be concluded that an error occurred during the reconstruction of this face. The considered cell, to which the face belongs, is near the border of the

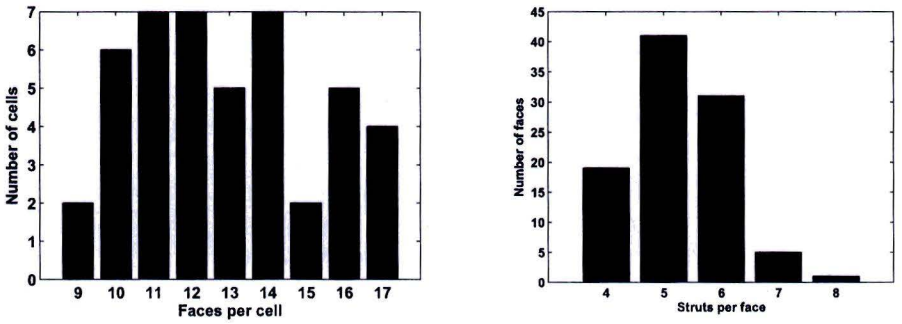

(a) (b)

Figure 19: The number of faces found per cell (a) and the number of struts found per face (b).

analyzed foam volume. It happens to be that one vertex of this cell lays outside the analyzed volume, see figure 20(a). Due to the limitations of the skeletonization algorithm at the boundaries of the volume, too many vertices are identified and the connectivity of the faces is reconstructed incorrectly, see figure 20(b). This also influences the surrounding faces. The correct reconstruction of faces is depicted in figure 20(c), which is done manually.

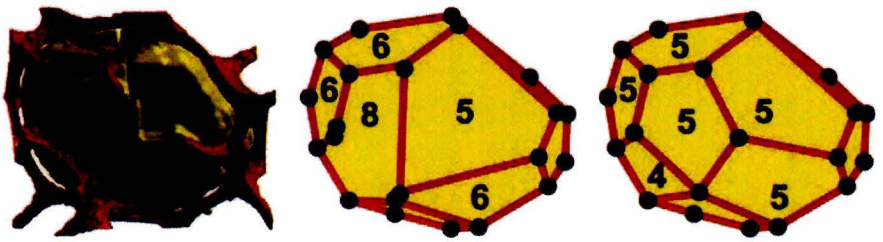

(a) (b) (c)

Figure 20: One vertex is outside the analyzed volume (a). The vertices are identified incorrect leading in an incorrect reconstruction of the faces. The number of struts per face is written on the faces (b). Manual reconstruction of the faces(c).

3.7 Discussion

In order to extract important foam properties, a 3D image of a piece of PUR foam was made using X-ray CT. The skeleton of the foam structure was computed. Using the computed skeleton, the strut length distribution and cross-sectional areas of the struts were obtained. A watershed segmentation of the air-bubbles, called cells, was computed. By examining the segmented cells, the cell morphology was analyzed resulting in properties like the cell volume, orientation and anisotropy. Also the number of faces per cell and the number of struts per face of the individual cells were obtained. These obtained foam properties will be used as input for a periodic finite element foam model, which will be discussed in the following chapter.

4 Periodic foam model

In order to model foams, it is convenient to create a periodic foam geometry. By using a periodic geometry it is possible to simulate a small domain. By doing this the numerical costs are kept low. The periodic foam model is created from a periodic skeleton, obtained from a 3D periodic Voronoi tessellation, where a 3D mesh is built around the struts of the skeleton.

4.1 Periodic Voronoi tessellation

Voronoi tessellation is used to create a 3D skeleton. This skeleton is used as a template to create a 3D finite element model of an open-cell foam. A Voronoi tessellation is a partition of space around a set of seeds. In 2D every partition of space is the area that is closest to a single seed and in 3D it is the volume of space closest to a single seed. In figure 21, a Voronoi tessellation of four seeds is depicted.

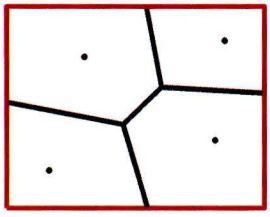

Figure 21: Voronoi tessellation of 4 random seeds.

A Voronoi tessellation can be made periodic by duplicating the original seeds to all adjacent regions. After applying the Voronoi tessellation, the center region, in which the original seeds are positioned, is now a periodic tessellation, as shown in figure 22 for the seeds of figure 21.

In figure 22(b) a rectangle is taken as the periodic region. By just taking a rectangular region it is possible that a vertex will lay on or near the boundary. By taking a rectangular region also the struts are cut at random angles. These features of a rectangular periodic region results in difficulties when placing a periodic mesh around the skeletons as described later on in section 4.5. Therefore the struts, which run through the faces of the rectangular periodic region are cut perpendicular at the center of these struts, as depicted in figure 22(c). Resulting in a periodic tessellation without straight boundaries, see figure 22(d).

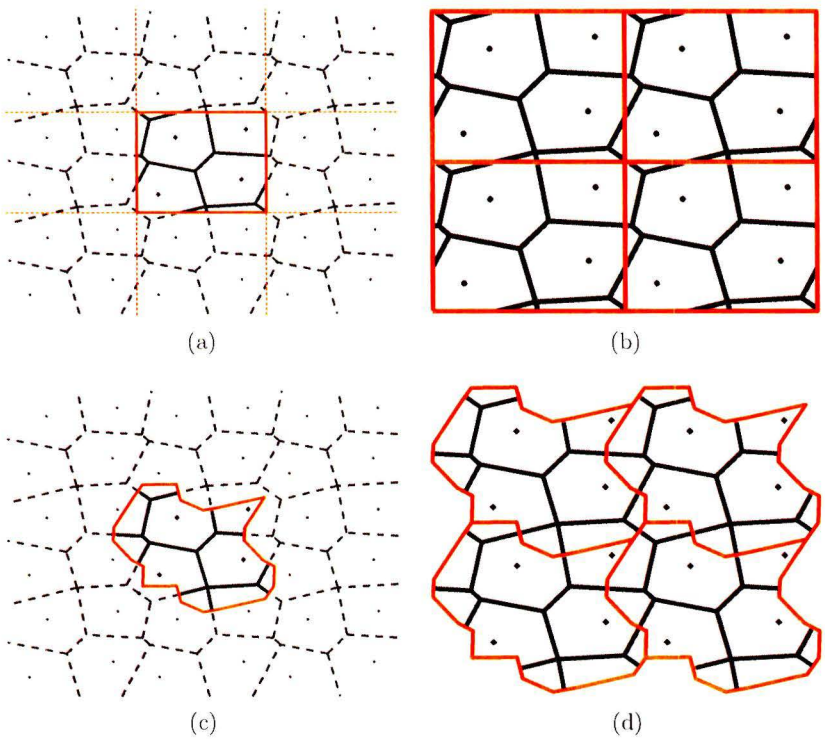

Figure 22: The four seeds, from figure 21, duplicated to the adjacent regions (a), and the resulting periodic tessellation (b). It is also possible to extract other periodic regions from the tessellation (c). Here the periodic boundaries run through the center of the struts (d).

A periodic foam model has the advantage that the finite element simulations can be conducted with periodic boundary conditions (PBC), which will be explained in section 4.6. PBC are useful in order to keep the finite element model small and thus keep computational costs low.

4.2 Kelvin cell

Lord Kelvin [10] proposed a tetrakaidecahedral cell to model the structure of three-dimensional open-cell foams, commonly called a Kelvin cell, see figure 23(a). The Kelvin cell almost minimizes surface area, which indicates that it is a good representative cell for open-cell foams. Each cell consist of six square and eight hexagonal faces and every edge has the same length. The edges meet at tetrahedral vertices and the cell centers are arranged according to a body centered cubic (BCC) lattice.

Zhu et al. [4] analytically showed that a Kelvin cell is almost isotropic. When the cross sectional area of the struts are triangular an elastic anisotropy factor of 0.964 was determined. This means that the Young's modulus $E_{[111]}$ is related to $E_{[100]}$ by:

$$E_{[111]} = \frac{27}{28} E_{[100]}. \tag{4}$$

Kelvin cells are obtained from the Voronoi tessellation of seeds placed on a BCC lattice. A representative volume element (RVE) describing the Kelvin cell is made by cutting the struts which run through the faces of the RVE in halve, see figure 23(b).

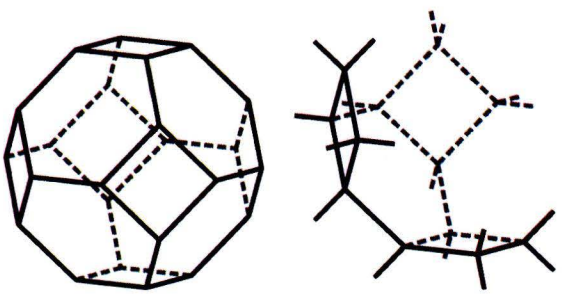

(a) (b)

Figure 23: A single Kelvin cell (a) and the periodic RVE describing a Kelvin cell.

4.3 Perturbated Kelvin cells

In order to create less regular foams the seeds of the Kelvin cells are perturbated before tessellation. The locations of seeds $\vec{S_0}$ placed on the BCC laticce are perturbated with a perturbation vector $\vec{p}$ by:

$$\vec{S_i} = \vec{S_0 i} + \vec{p_i}, \tag{5}$$

where $\vec{p_i}$; has an approximately random direction and a uniform distributed amplitude ranging between preset values.

By applying a Voronoi tessellation to the set of perturbed seeds $\vec{S}$ a more random cellular structure is obtained which, depending on the amplitude of $\vec{p_i}$, varies between Kelvin cells and a random Voronoi structure. When more random Voronoi structures are considered, the morphology of the cells changes as depicted in figure 24. Cells with 5 struts per face are present in the foam structures perturbed with an amplitude of 0.2 mm, see the pink cell in figure 24(c).

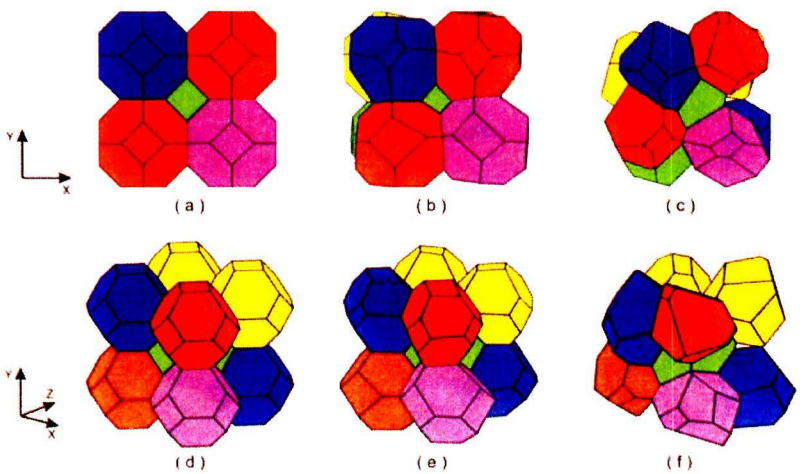

Figure 24: Kelvin cells (a), (d), Kelvin cells perturbated with $|\vec{p}| = 0 - 0.1$ mm (b), (e) and Kelvin cells perturbated with $|\vec{p}| = 0 - 0.2$ mm (c), (f).

The strut length distribution changes from a uniform strut length in the Kelvin cell, to a distribution similar as in real foams to a distribution common for random Voronoi tessellations, as depicted in figure 25. All three distributions have a mean strut length of 0.29 mm.

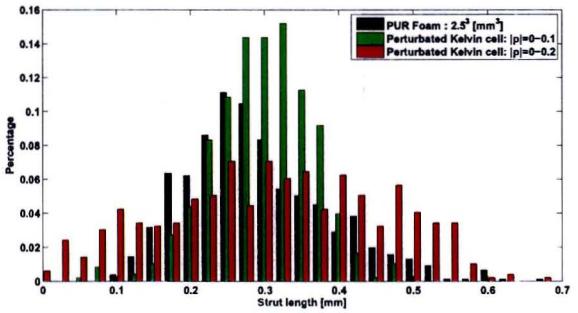

Figure 25: Strut length distribution found in a real foam and in perturbated Kelvin cell tessellations.

4.4 Anisotropic Kelvin cells

As described in section 3.6, the cells found in the examined PUR foam have an ellipsoidal shape, and are therefore anisotropic. The ratio between the major-axis and the two minor-axes is obtained. The mean ellipse-ratio is used as an input to affinely stretch the skeletons of the Kelvin cells and perturbated Kelvin cells. One direction is multiplied by the ellipse-ratio and the other two directions are divided by the ellipse-ratio in order to obtain orientated anisotropic cells, as depicted in figure 26.

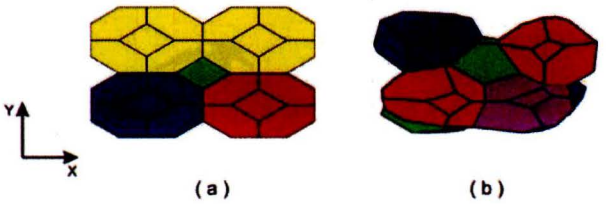

Figure 26: Affinely stretched Kelvin cells (a) (c) and affinely stretched Kelvin cells perturbated with $|\vec{p}| = 0 - 0.2$ mm (b) (d)

4.5 Mesh generation

As shown in section 3.4 the ligaments of the foam are of triangular shape and the cross section of the ligament changes along the length of the ligament.

The Voronoi tessellation is a vertex-strut representation of the foam. In order to make a mesh, beams with equilateral triangular cross sections are meshed around the struts of the tessellation. The mid section areas A_0 of the struts are obtained from the data depicted in figure 12 and are given by:

$$\begin{aligned} A_0(0.1\,\text{mm} < L < 0.4\,\text{mm}) &= -0.0874L^3 + 0.1171L^2 - 0.0507L + 0.0086 \\ A_0(L > 0.4\,\text{mm}) &= A_0(L = 0.4\,\text{mm}) \end{aligned} \tag{6}$$

where L is the length of the strut considered. The faces of the equilateral triangle, placed around the struts, are oriented by the unit face normals $\vec{N}_i$, with $i = 1, 2, 3$, such that the sum of the angles between the face normals and the in-plane vectors towards the corresponding cell centra $\vec{C}_i$ of the neighboring cells is as small as possible, see figure 27(a). The vectors $\vec{t}_i$ describe the distance and direction of the points on the edges of the triangular strut to the center of the strut. The variation in strut cross section is also described by $\vec{t}_i$ by:

$$\vec{t}(\xi, A_0)_i = -\left(0.0043\xi^2 - 0.0043\xi + \sqrt{\frac{4A_0}{3\sqrt{3}}}\right) \cdot \vec{N}_i \tag{7}$$

where ξ is the normalized strut length ranging between -1 and 1, so that when $\xi = 0$ the vectors $\vec{t}_i$ span the area A_0. The vectors $\vec{t}_i$ are used to place nodes around the skeleton struts obtained from the Voronoi tessellation. In figure 27(b) the geometry of a single strut is visualized.

The mesh generation is explained here. First, al nodes are placed around the skeleton struts obtained from the Voronoi tessellation, see figure 28(a). Then all nodes which lie close to each other in the vertices are swept and a Delaunay triangulation is computed resulting in a convex tetrahedron mesh. Therefore, a simple rejection method is written to delete large tetrahedrons resulting in a concave mesh, see figure 28(b). The rejection method is based on the fact that the dimensions of the elements in the desired mesh are known. In the vertices some additional elements are automatically added by the Delaunay triangulation. However these 'extra' elements are not undesired. The way these vertices are meshed greatly resembles vertices found in a real foam structure, as can be seen in figure 29(a) and (b). The amount of extra added elements in the vertices is dependent on number of struts and the angle between these struts. Sharp angles create more additional elements, as can be seen in figure 29(c). Here six struts meet at a single vertex, and additional elements are placed between the upper two struts which meet at a sharp angle, resulting in an un-realistic vertex.

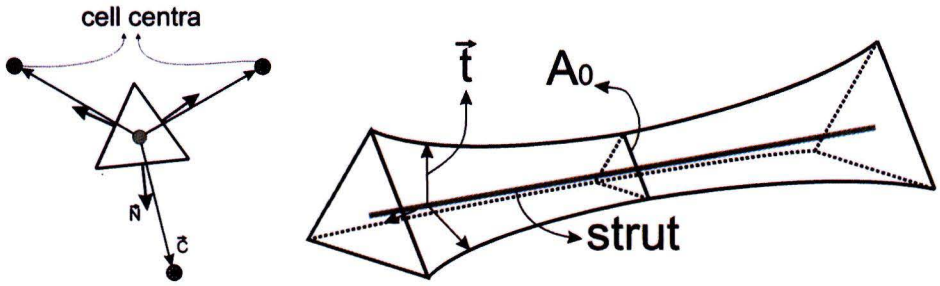

Figure 27: The faces of the triangular struts are placed in such a way that the sum of all angles between the face normals $\vec{N}$ and the vectors pointing towards the cell centra $\vec{C}$ surrounding a strut is as small as possible (a). A representation of the geometry of a strut after meshing the skeleton struts (b).

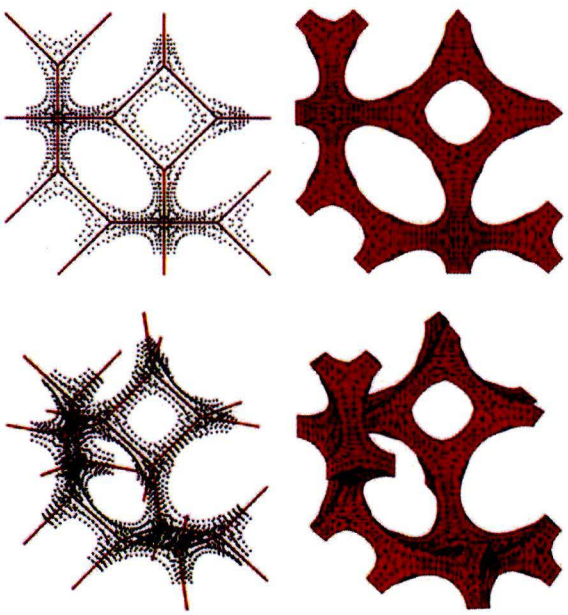

Figure 28: Nodes placed around the foam skeleton (a). After deleting specified tetrahedrons the concave foam mesh is obtained (b).

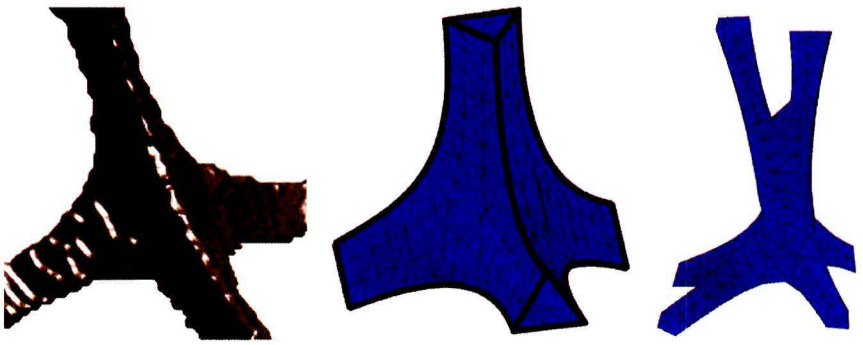

(a) (b) (c)

Figure 29: A vertex extracted from the PUR foam (a), a realistic vertex as modeled in the finite element mesh (b), and a un-realistic vertex as modeled in the finite element mesh (c).

The mesh of the Kelvin cell contains out of approximately 12.000 tetrahedrons. Mentat is used to convert the linear tetrahedrons into quadratic tetrahedrons.

4.6 Periodic boundary conditions

The foam is subjected to periodic boundary conditions (PBC). In figure 30(a) a 2D view of the PBC is given. Since there are not always physical nodes on the corners of the RVE, the dummy nodes D_i, with $i = 1, 2, 3, 4$, are used to prescribe displacements or loads onto the RVE. The dummy nodes are nodes which lie freely at the corners of the RVE, thus without being attached to any finite element [15]. In figure 30, the black box represents the RVE, the gray struts represent the struts at the boundary faces, the red lines represent the periodic links between the struts and the black dots represent the dummy nodes. The PBC are written as:

$$\vec{u}_R = \vec{u}_L + \vec{u}_{D2} - \vec{u}_{D1} \quad (8)$$

$$\vec{u}_T = \vec{u}_B + \vec{u}_{D3} - \vec{u}_{D1} \quad (9)$$

$$\vec{u}_F = \vec{u}_A + \vec{u}_{D4} - \vec{u}_{D1} \quad (10)$$

$$\vec{u}_{RT} = \vec{u}_{LB} + \vec{u}_{D2} + \vec{u}_{D3} - 2\vec{u}_{D1} \quad (11)$$

$$\vec{u}_{RF} = \vec{u}_{LA} + \vec{u}_{D2} + \vec{u}_{D4} - 2\vec{u}_{D1} \quad (12)$$

$$\vec{u}_{TF} = \vec{u}_{BA} + \vec{u}_{D3} + \vec{u}_{D4} - 2\vec{u}_{D1} \quad (13)$$

where $\vec{u}$ are displacements and the subscript indicates the nodes which are prescribed: **R**ight, **L**eft, **T**op, **B**ottom, **F**ront, b**A**ck and the **D**ummy nodes **1-4**.

The boundary conditions are depicted in figure 30(b), where uniaxial compression in the y-direction is depicted. The displacement node D_1 is fixed in all directions, D_2 is fixed in y-direction, D_3 is fixed in y- and z-direction and an displacement is applied to D_4. In this manner the foam sample is free to contract.

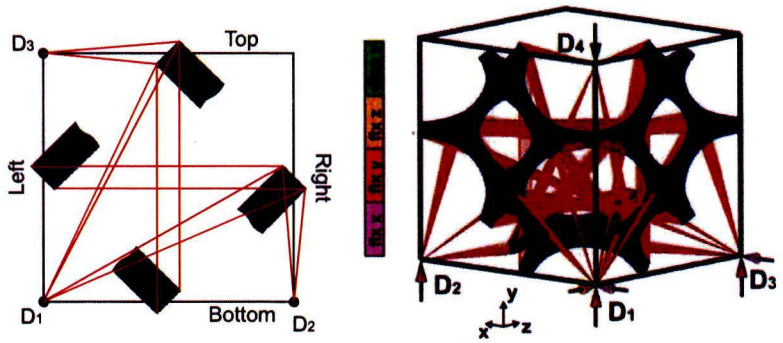

(a) (b)

Figure 30: 2D representation of the periodic boundary conditions (a) and the boundary conditions describing uniaxial compression (b).

4.7 Material model

The EGP model [9] is used as a constitutive model to describe the PUR material. The stress-strain response for a rejuvenated polymer is depicted in figure 31. To properly describe glassy polymers, a distinction is made between the contribution of secondary interactions between polymer chains, which cause the (visco-)elastic properties at small deformations, and the entangled polymer network which governs strain hardening. This decomposition is described as follows:

$$\boldsymbol{\sigma}(\dot{\varepsilon}, S, \varepsilon) = \boldsymbol{\sigma}_s(\dot{\varepsilon}, S) + \boldsymbol{\sigma}_r(\varepsilon) \tag{14}$$

where $\boldsymbol{\sigma}$ is the Cauchy stress, $\boldsymbol{\sigma}_s$ is the driving stress and $\boldsymbol{\sigma}_r$ the hardening stress. The driving stress $\boldsymbol{\sigma}_s$ is given by:

$$\boldsymbol{\sigma}_s(\dot{\varepsilon}, S) = \boldsymbol{\sigma}_{rej}(\dot{\varepsilon}) + \Delta\boldsymbol{\sigma}_y(S) \tag{15}$$

where $\boldsymbol{\sigma}_{rej}(\dot{\varepsilon})$ is the history independent rejuvenated stress and $\Delta\boldsymbol{\sigma}_y(S)$ the history dependent transient yield drop [16]. In this work the history parameter S is set to zero, so the the history dependent transient yield drop $\Delta\boldsymbol{\sigma}_y(S)$ is not taken into account. The hardening stress $\boldsymbol{\sigma}_r$ is given by:

$$\boldsymbol{\sigma}_r(\varepsilon) = G_r \tilde{\boldsymbol{B}}^d \tag{16}$$

where G_r is the strain hardening modulus and $\tilde{B}^d$ the deviatoric part of the isochoric left Cauchy-Green deformation tensor.

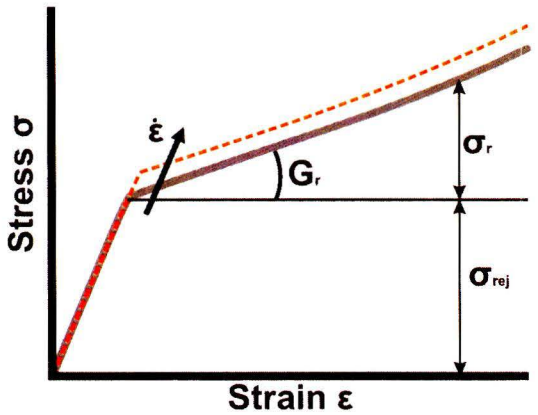

Figure 31: Schematic stress-strain response of the EGP model for the rejuvenated state and a decomposition of the Cauchy stress in two separate stress contributions: the rejuvenated stress $\boldsymbol{\sigma}_{rej}$ and the hardening stress $\boldsymbol{\sigma}_r$. The slope G_r is the strain hardening modulus.

4.8 Discussion

As shown in section 3.6, the mean number of faces per cell equals 12.9 and the number of struts per face equals 5.25 in the examined piece of PUR foam. Most faces in the considered PUR foam consisted of 5 struts. The Kelvin cell on the other hand has no faces consisting of 5 struts and has 14 faces. However previous studies indicated that the Kelvin cell is an adequate space filling cell structure in order to model open-cell foams [6].

A more random foam structure with a wider strut length distribution and cell size distribution is created by perturbing Kelvin cells. The strut length distribution of these less regular foams shows good comparison with the strut

length distribution as found in the examined PUR foam. In these less regular foam structures, faces consisting of 5 struts do occur, as can be seen in figure 24(c) and (f). Thus the influence of cell morphology can also be investigated using these less regular foam structures.

In chapter 3.6, it was shown that the cells, in the examined PUR foam, have an anisotropic geometry and are orientated in one direction. By affinely stretching the Kelvin cells and perturbed Kelvin cells, this foam feature is also introduced in the periodic foam models. The influence of anisotropy can be studied with these anisotropic foam models.

5 Results

In this section the results of the simulations are discussed and compared with a reference experiment and simulations. The compression behavior of increasingly less regular foam structures is investigated. The volumetric response of a Kelvin cell in compression and tension is also examined.

5.1 Reference experiment and simulations

In order to obtain a reference for the simulations, an experiment is carried out on the same PUR foam sample as was used for the image analysis as described in chapter 3. The dimensions of the foam sample and the strain rate are given in table 1. Compression is applied. The experimental procedure and conditions are further described in the work of Wismans [8]. The stress-strain response obtained is shown in figure 32. First, an elastic regime is visible, followed by a plateau stress.

Table 1: Sample dimensions

	Sample volume [mm^3]
Experiment	$\pi \times 29.25^2 \times 32.5 = 8.7 \times 10^4$
Simulation	$4 \times 4 \times 4 = 64$

Three simulations carried out by Wismans are also used as a reference. These reference simulations are performed with a mesh which is directly made from the scanned micro structure of the PUR foam used for the experiment. The EGP model is used for the polymer material, see table 2. Three reference simulations are carried out, where uniaxial compression between two plates is applied in the x-, y- and z-direction. Symmetry boundary conditions are used, as described in Wismans [8].

In the simulated mechanical response, also an initial elastic regime is observed, followed by a plateau stress. The plateau is induced by the visco-plastic material behavior creating plastic hinges in the foam. The reference simulations clearly show the anisotropic properties of the PUR foam, as described in section 3.5 and shown in figure 32. The stiffness of the foam is more or less the same when compressed in the y- and z-direction, but the stiffness of the PUR foam is significantly higher when compressed in the x-direction.

The reference experiment and simulations are in good agreement. The direction of compression, applied in the reference experiment, is perpendicular to

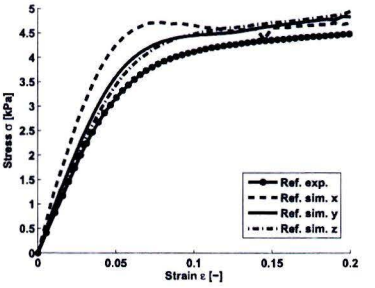

Figure 32: Reference experiment and the reference simulations.

the cell orientation in the foam sample. Therefore, the response of the experiment is in agreement with the reference simulations in y- and z-direction.

The plateau stress is a bit higher in the reference simulations than in the reference experiment. A possible explanation is that the considered volume of the reference simulations is too small. Another explanation is that the material properties, used in the reference simulations and given in table 2, are not precise enough.

5.2 Kelvin cell

First, a Kelvin cell is used to model the mechanical response of the PUR foam. As explained in section 4.2, a Kelvin cell is a cell structure widely used in literature to simulate the mechanical behavior of foams. Here, a fully three-dimensional mesh of a Kelvin cell with a Mooney-Rivlin material model is made. The material properties can be found in table 2. The variables of the mesh are the strut length, which automatically correlates which the cell volume, the mid area of the strut and thickness variation of the cross sectional area. The strut thickness correlates with the relative density of the foam. The struts of the Kelvin cell have a triangular cross sectional area without a Plateau border. All properties are summarized in table 3.

The Kelvin cell is subjected to uniaxial compression and the global stress-strain diagram is depicted in figure 33. The Kelvin cell responds with an increasing stress, without a clear distinction between an initial elastic region and a plateau stress. No buckling of struts is present because the geometry is symmetrical. The deformed mesh and the resulting von Mises stress are depicted in figure 34(a). The stress concentrates in the struts near the vertices. As can be seen in the cross sectional slice of the struts, as depicted

Table 2: The bulk modulus κ, shear modulus G and hardening modulus G_r which are used in the material models.

	κ [MPa]	G [MPa]	G_r [MPa]	τ_0	η_0	S_0	μ
EGPM	30	140	2.6	0.07	$3{\cdot}10^{10}$	0	0.08
Mooney-Rivlin	30	140	-	-	-	-	-

Table 3: The mid area of the struts A_0, strut length L, relative density ϕ and volume of the Kelvin cell

	A_0[mm^2]	L [mm]	ϕ	volume [mm^3]
Kelvin cell	0.0017	0.29	0.031	0.2759

in figure 34(a), the peak stress is located in the point of the triangular cross section which points in the direction of compression.

The response of the Kelvin cell is also obtained using the EGP model. The material properties are summarized in table 2. The global stress-strain diagram is depicted in figure 33. The initial response is slightly stiffer than the Mooney-Rivlin model followed by a slightly stiffer response. This is due to the hardening in the edges of the struts. In this simulation, a clear distinction between an elastic region and a plateau stress is visible. The visco-plastic material behavior results in plastic regions in the struts, resulting in more uniform stress distribution in the struts, see figure 34(b). These regions form near the vertices of the foam creating plastic hinges. There is no buckling present in this simulation because the geometry is symmetrical.

From these two simulations, it can be concluded that the combination of the micro-structure and a proper material description is essential to describe the mechanical response of foams. In comparison to the reference simulations, where the material description and the micro-structure are considered "perfect", it is shown that a very simple micro-structure with a good description of the material yields quantitatively good results. However the initial stiffness and plateau stress are too high.

5.3 Plateau border

In chapter 3.4, the cross section of the struts was examined. Here, a Plateau border was observed in the cross sectional area of the struts as also described

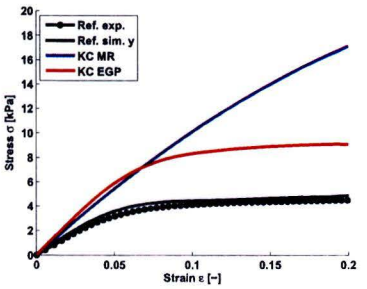

Figure 33: The stress-strain response of a Kelvin cell (KC) with the Mooney-Rivlin (MR) and the EGP material model.

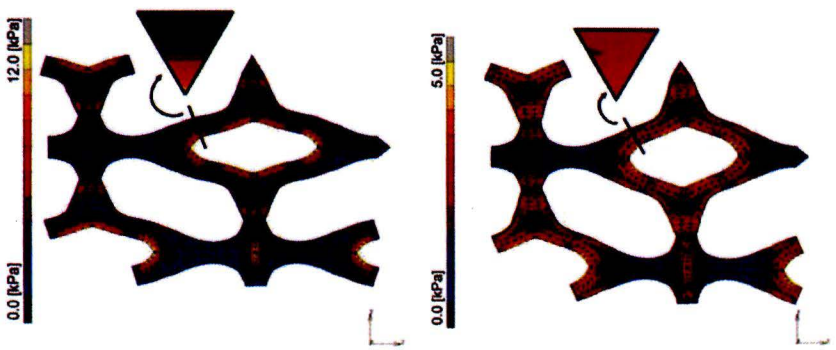

(a) (b)

Figure 34: Equivalent von Mises stress field of a Kelvin with a Mooney-Rivlin material model (a) and the EGP model (b) compressed in the vertical direction. Cross sections of the triangular struts are depicted.

by [6]. To investigate the influence of such a Plateau border, the Kelvin cell, as described in section 5.2, is given a Plateau border cross section with the same area, see figure 35. The stress-strain diagram of the simulation is depicted in figure 36.

The response of the model which includes the Plateau border is stiffer and stronger than the model without the Plateau border cross section. After a strain of 0.15, the model which includes the Plateau border shows a clear softening. This softening behavior is because the geometry is not perfectly symmetric, due to the meshing method of the vertices, and the struts of the Kelvin cell start to buckle.

The initially stiffer response can be explained by the fact that the second moment of inertia of the Plateau border is larger than the second moment of inertia of the triangular cross section. Keeping this in mind, the modeling of the plateau border is not included in further simulations.

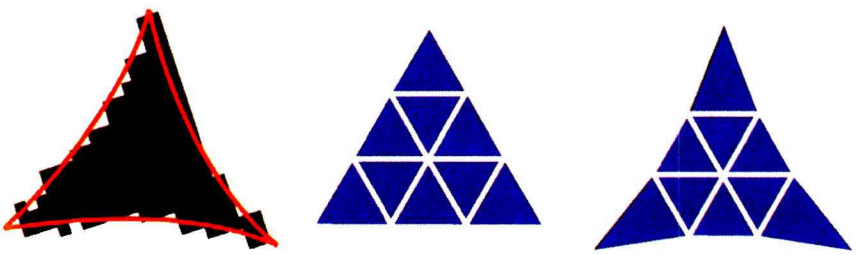

(a) (b) (c)

Figure 35: The cross sectional area of the struts in the CT measurements of the foam, where (a) shows the cross section as found in the foam, (b) the cross section as meshed without a Plateau border and (c) a cross section with the same area as (b) but with a Plateau border.

5.4 Perturbed Kelvin Cells

A Kelvin cell is a perfectly symmetrical representation of a foam structure. However as described in chapter 4.2 these cells are not commonly found in real foams. Therefore, to obtain a more random foam, perturbed Kelvin cells are created as described in section 4.3. The simulations performed on these geometries use the EGP model as a material model because of the importance

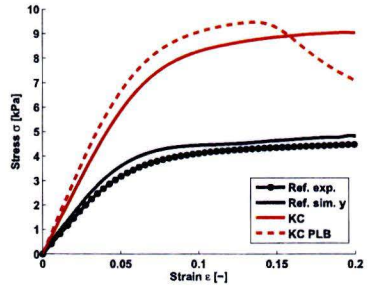

Figure 36: The stress-strain curves of a Kelvin cell (KC) without and with a Plateau border (KC PLB).

of using a proper constitutive description and no Plateau border is included, as discussed above.

Several models, with different amplitude of perturbation $\vec{p}$, are created in order to investigate the influence such a perturbation of a grid of Kelvin cells on the response, see table 4. The stress-strain response is depicted in figure 37(a). Due to the method of meshing, the geometry the relative density increases with larger amplitude of perturbation $\vec{p}$. This larger relative density is the reason for the increasing stiffness. The elastic responses of the perturbed foams are scaled by the relative density ϕ times the Young's modulus of PUR E_s, according to equation (2). The scaled elastic responses are now approximately equally stiff, see figure 37(b). The fact that the perturbed foams have a wider distribution of strut lengths does not influence the initial scaled stiffness of the foam. It is shown that the Kelvin cell and the perturbed foams have a too stiff elastic response in comparison with the reference stress-strain responses.

Table 4: The details of the different simulations are given here: simulation name, number of cells, relative density ϕ and the amplitude of the perturbation vector $\|\vec{p}\|$.

	No. of cells	ϕ	Perturbation $\|\vec{p}\|$ [mm]
KC	$1 \times 1 \times 1 = 1$	0.031	none
8 KC p=0.1	$2 \times 2 \times 2 = 8$	0.031	0.1
16 KC p=0.1	$4 \times 4 \times 1 = 16$	0.031	0.1
8 KC p=0.2	$2 \times 2 \times 2 = 8$	0.036	0.2
16 KC p=0.2	$4 \times 4 \times 1 = 16$	0.036	0.2

However, the perturbations do create weak spots in the foam, which leads to local buckling of some struts resulting in a lower plateau stress, see figure 37. The buckling of some struts leads to a collapse band which runs, more or less, horizontal through the foam, see figure 38(c) and (d). The PBC enforce the horizontal localization bands, because the localization band has to be periodic as well.

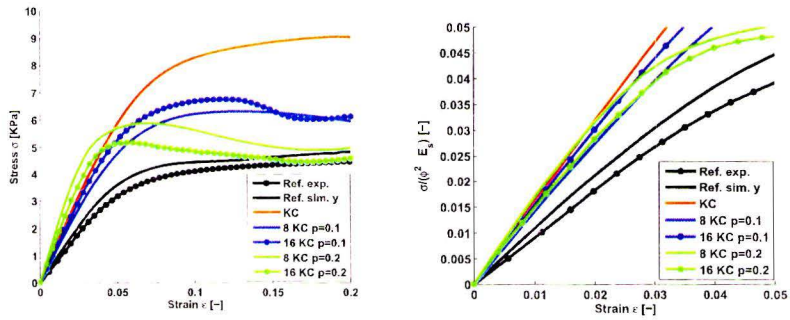

(a) (b)

Figure 37: The stress-strain responses of perturbed Kelvin cells with different amplitude of perturbation and different number of cells(a) and the scaled elastic responses (b).

5.5 Kelvin cell: anisotropy

A Kelvin cell represents an isotropic foam [4]. However, as discussed in section 3.5, the cells in the examined PUR foam are anisotropic and orientated. Therefore, an affine stretch is applied to the geometry of the Kelvin cell to obtain an anisotropic cell. The anisotropic Kelvin cell is subsequently compressed in x- and y-direction, see figure 39. As can be seen, a clear difference in responses between the x- and y-direction is visible. Whereas the y-direction has a response which is in good agreement with the reference simulation, the x-direction is much stiffer. An explanation for these findings can be that when compressing in the x-direction, the orientation of the single anisotropic Kelvin cell is perfectly in line with the applied compression, which makes it very stiff. In a real foam the orientations of the cells are not perfectly aligned, and therefore the big difference in response in different directions is much smaller.

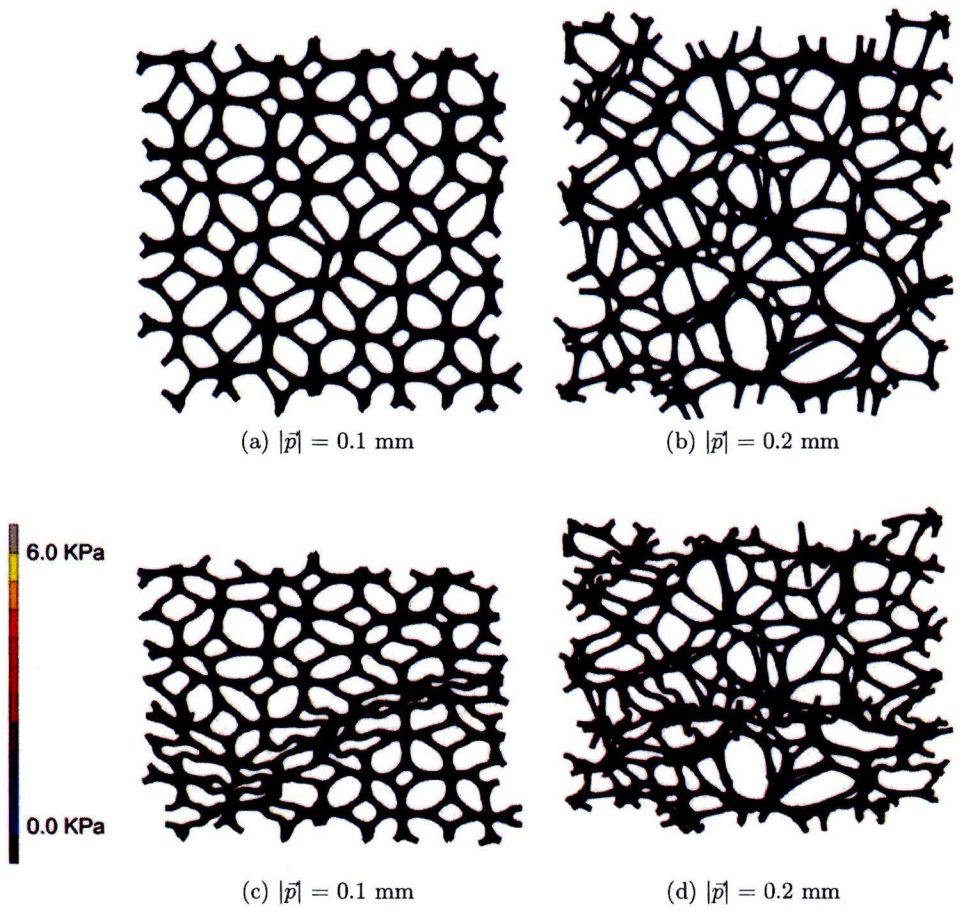

(a) $|\vec{p}| = 0.1$ mm (b) $|\vec{p}| = 0.2$ mm

(c) $|\vec{p}| = 0.1$ mm (d) $|\vec{p}| = 0.2$ mm

Figure 38: The undeformed meshes (a) & (b) and deformed meshes (c) & (d) for different amplitudes of perturbation $\vec{p}$. The von Mises stresses are depicted.

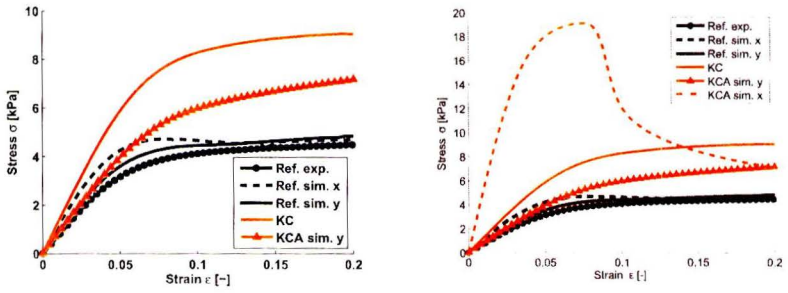

(a) (b)

Figure 39: Response of the anisotropic Kelvin cell (KCA) loaded in the y-direction (a) and loaded in x-direction (b).

The anisotropic Kelvin cell which is compressed in the x-direction shows an extreme softening. Again this is because the geometry is not perfectly symmetrical due to the meshing method. A slight imperfection in the mesh results in buckling of the struts leading to this softening.

5.6 Anisotropic perturbed Kelvin cells

The anisotropic Kelvin cell is also perturbed to investigate the influence of irregularities in the foam structure, see table 5. The results are depicted in figure 40(a) and (b). The same conclusions can be made as in section 5.4. By creating a more random foam, weak spots are present in the foam which lead to a lower plateau stress. A perturbation $\vec{p}$ with an amplitude of 0.2 yields good results when compared with the reference simulations for loading in the y-direction. However, when loaded in the x-direction, the response is still too stiff and the plateau stress is too high. The most likely explanation is that the orientation of the anisotropy in the simulated foams is too perfect, leading to perfectly aligned struts in the direction of compression. Whereas the magnitude of anisotropy found in the real PUR foam is accounted for, the distribution of this orientation is not taken into account in these simulations.

Table 5: The details of the different simulations are given here: simulation name, number of cells, relative density ϕ and the amplitude of the perturbation vector $\|\vec{p}\|$.

	Nr. cells	ϕ	Perturbation $\|\vec{p}\|$ [mm]
KCA	$1 \times 1 \times 1 = 1$	0.031	none
9 KCA p=0.1	$3 \times 3 \times 1 = 9$	0.031	0.1
9 KCA p=0.2	$3 \times 3 \times 1 = 9$	0.033	0.2
27 KCA p=0.2	$3 \times 3 \times 3 = 27$	0.033	0.2

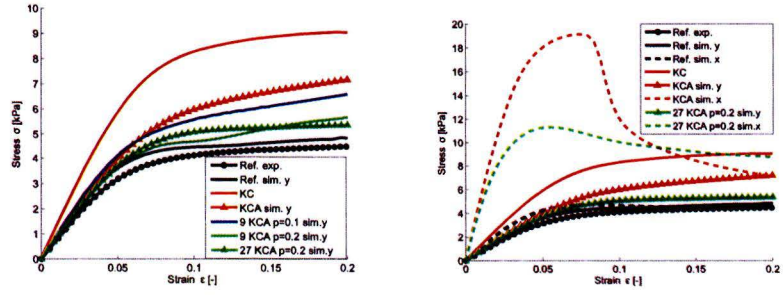

(a) (b)

Figure 40: Response of a perturbed anisotropic Kelvin cell loaded in the y-direction (a) and also loaded in x-direction (b).

5.7 Volumetric response of open-cell foams

As was shown by the numerical simulations of Wismans [8], the volumetric response J, given by:

$$J = V/V_0 \tag{17}$$

of open-cell foams is remarkable, as depicted in figure 41. In compression, the volume decreases as expected. However, in tension a small increase in volume is observed followed by an decrease in volume. It was shown by Wismans that the transverse orientated struts in the foam start to buckle, resulting in a decrease in macroscopic volume of the foam.

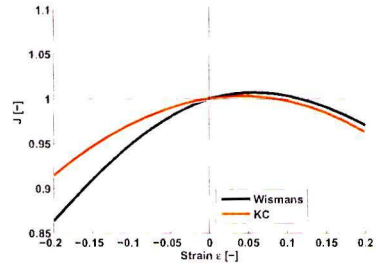

Figure 41: The volumetric response of a Kelvin cell (KC) and the volume response of a realistic foam model [8].

The results of Wismans are compared with the volumetric response of a Kelvin cell. The quantitative volumetric response of the Kelvin cell is similar to the volumetric response observed by Wismans. The deformed states of the Kelvin cell in compression and tension are depicted in figure 42. In tension, the diagonally orientated struts bend in an S-shape, which results in a decrease of macroscopic volume of the foam. The struts which are orientated perfectly perpendicular to the tensile direction do not deform.

The volumetric response is also computed for two perturbed foam structures, an anisotropic Kelvin cell and a perturbed anisotropic foam structure, see figure 43. The volume response for the perturbed foam structures does not seem to improve compared with the volume response of the Kelvin cell. The overall shape is quantitatively the samen, but qualitatively the volumetric response does not improve. When considering the volume response of the anisotropic foam structures it can be concluded that the response in strain is not representative for real foams. The anisotropic foam models are too stiff in the x-direction, see figure 44. When stretching the anisotropic cells in the

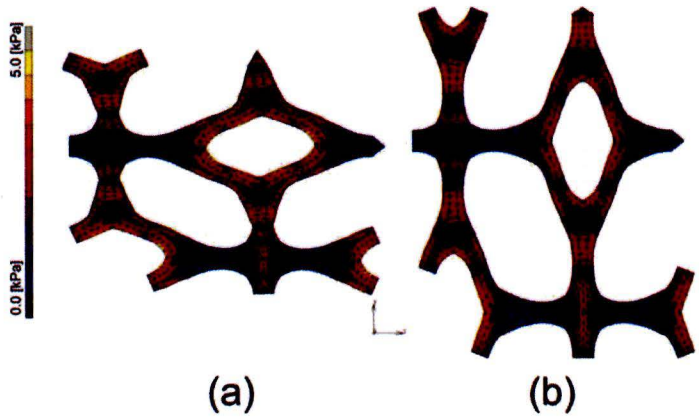

Figure 42: The deformed compressed Kelvin cell (a) and the deformed stretched Kelvin cell (b). The von Mises stress field is plotted.

y-direction, the contraction in x-direction is too small for a drop in global volume.

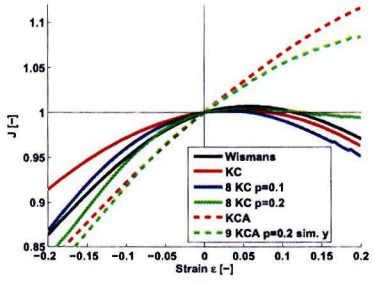

Figure 43: The volumetric response of a Kelvin cell (KC), the volume response of a realistic foam model [8], of two perturbed models, a anisotropic Kelvin cell (KCA) and perturbed anisotropic Kelvin cells.

5.8 Discussion

By investigating increasingly less regular foam structures, the important features of the micro-structure are obtained. The most important foam characteristics in the elastic region are the relative density ϕ, the cross sectional area of the struts, cell shape and cell orientation. These properties are important

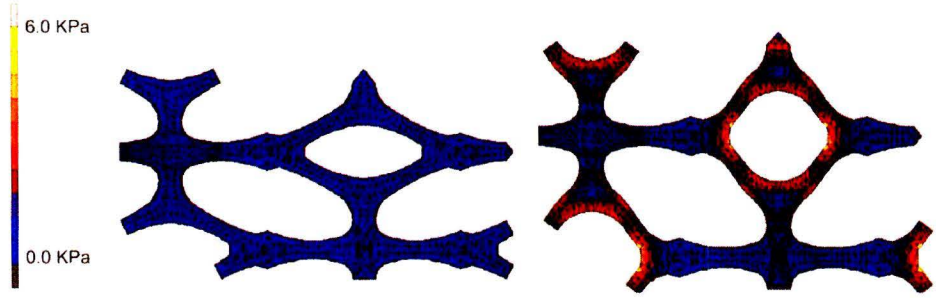

(a) (b)

Figure 44: The undeformed anisotropic Kelvin cell (a) and the stretched anisotropic Kelvin cell (b). The von Mises stress is depicted here.

when considering the stiffness of the foam.

The amplitude of the plateau stress is governed by the weaker regions in the foam, the cross sectional area of the struts, cell shape and orientation. When the regularity of a foam structure decreases, the variation in strength throughout the volume of the foam increases, resulting in weak spots where buckling of struts initiates earlier. Hence, a lower plateau stress is the result. The cross sectional area also influences the strength of the foam. Stronger struts lead to a higher plateau stress.

The volumetric response of a Kelvin cell quantitatively describes the volumetric response of foams very well. The volume decreases in compression, increases with small tensile strains and decreases again when larger tensile strains are applied.

6 Conclusion

The micro-structure of a PUR foam was examined. X-ray CT was used to obtain 3D images and image analysis was performed in order to extract important foam properties from these images. The skeleton of the foam structure was computed. Using the computed skeleton, the strut length distribution and cross-sectional area of the struts was obtained. A watershed segmentation of the air-bubbles, called cells, was computed. By examining the segmented cells, the cell morphology was analyzed, resulting in properties like the cell volume, orientation and anisotropy. Also the number of faces per cell and the number of struts per face of the individual cells were obtained.

A periodic foam geometry was created using a periodic Voronoi tessellation. The struts obtained from the tessellation were used as a template for a 3D finite element mesh consisting of quadratic tetrahedrons. The tetrahedrons, containing four nodes, were placed using a 3D Delaunay triangulation, and converted into quadratic tetrahedrons afterwards.

To investigate the importance of the different foam characteristics, increasingly less regular foam structures were created. The Kelvin cell was the most regular foam examined. The mean cell volume, strut thickness and change in cross sectional area were the input for the 3D geometry of the Kelvin cell. The volumetric response and mechanical response were computed and compared with a reference experiment and simulations. It was shown that a proper intrinsic material description was very important to properly describe open-cell PUR foams. The geometry of a Kelvin cell quantitatively shows similar response as the references, for both the volumetric and the mechanical response. However, qualitatively, the Kelvin cell was a too simple representation. The influence of a Plateau border cross sectional area was investigated, resulting in an overall stiffer and stronger response.

A more random foam structure with a wider strut length distribution and cell size distribution was created by perturbing Kelvin cells. The strut length distribution of these less regular foam compared well with the strut length distribution as found in the examined PUR foam. Also the foam morphology of these structures show better agreement with real PUR foams. However, the elastic response remains more or less the same as for regular Kelvin cells. The plateau stress decrease, because there were weaker regions present in the foam.

By affinely stretching regular Kelvin cells and perturbed volumes of Kelvin cells, the influence of cell shape and orientation was investigated. The mechanical response, of these anisotropic foam structures, was in very good

agreement with the reference experiment and simulation when compression is applied perpendicular to the cell orientation. When the compression direction is aligned with the cell orientation, the mechanical response was far too stiff. This too stiff response can be due to the perfect alignment of all cell orientations with the direction of applied compression.

The most important foam characteristics in the elastic region were the relative density ϕ, the cross sectional area of the struts, cell shape and cell orientation. These properties were important when considering the stiffness of the foam.

However, when considering the amplitude of the plateau stress, the variation of strength throughout the foam plays an important role. When the regularity of a foam decreases, weak spots arise which initiates local buckling of struts. Hence, a lower plateau stress is the result. Of course, the strut thickness, cell shape and orientation play an important role as well in the height of the plateau stress. Stronger struts and cells lead to a higher plateau stress.

The volume response of the Kelvin cell did quantitatively described the volume change as found in real foams. However qualitatively it did not describe the volume response sufficiently. The less regular foam models showed similar results, were the quantitatively volume response was good, but qualitatively not. The anisotropic foam models did not correctly describe the volume response which is typical for real foams.

7 Recommendations

A Kelvin cell was used as a starting point in this work. However the morphology of a Kelvin cell does not compare well with most cells found in a real PUR foam. Another periodic cell structure which resembles the morphology of PUR foam more is a Weaire-Phelan structure. It could be interesting to investigate this structure as well.

In the Kelvin cell and the less regular foam structures, the struts do not meet at 109.8° in vertices. In the Kelvin cell only angles of 90° and 120° are present and in the less regular foams even sharper angles are not uncommon. An improvement can be made here in creating foam models. Jang et al. [6] used a program called "surface evolver", among other techniques and purposes, to create vertices with more realistic angles between struts. However, it could be possible to use other techniques to solve these problems.

In this work, Voronoi tessellation is used to create foam templates. It could be useful to use a weighted Voronoi tessellation in order to create a periodic foam. A weighted Voronoi tessellation takes into account cell size information from single seeds. Making it possible to create foam structures with a wider distribution of cell sizes [6]. The original cell centers, obtained from the CT-scan, can be used as seeds for the (weighted) Voronoi tessellation.

Affinely stretching the isotropic foam models to create a anisotropic foam model results in a too stiff response in the direction of stretching. Another manner to introduce anisotropy should be implemented in order to properly model anisotropic foam models.

References

[1] Z. Liu and M. G. Scanlon, *Predicting mechanical properties of bread crumb*, Trans IChemE, Vol 81, Part C, September (2003).

[2] L.J. Gibson and M.F. Ashby, *Cellular Solids, Structure and properties*, Second ed. (1999).

[3] T. Dillard, F. N'Guyen, E. Maire, L. Salvos, S. Forest, Y. Bienvenu, J.D. Bartout, M. Croset, R. Dendievel, P. Cloetens, *3D quantitative image analysis of open-cell nickel foams under tension and compression loading using X-ray microtomography*, Philosophical Magazine, Vol. 85, No. 19 (2005) 2147-2175.

[4] H.X. ZHU, J.F. Knott, N.J. Mills *Analysis of the elastic properties of open-cell foams with tetrakaidecahedral cells*, Journal of Mechanics and Physics os Solids, Vol. 45, No. 3 (1997) 319-343.

[5] Y. Takahashi, D. Okumura, N. Ohno *Yield and buckling behavior of Kelvin open-cell foams subjected to uniaxial compression*, International Journal of Mechanical Sciences, 52 (2010) 377-385.

[6] W.Y. Jang, S. Kyriakides, A.M. Kraynik, *On the compressive strength of open-cell metal foams with Kelvin and random cell structures*, International Journal of Solids and Structures, 47 (2010) 2872-2883.

[7] K.A. Brakke *The Surface Evolver*, Exp. Math. 1 (1992), 141-165 ¡http://www.susqu.edu/brakke/evolver/evolver.html¿.

[8] J.G.F Wismans *Computed tomography-based modeling of structured polymers*, Technische Universiteit Eindhoven (2011).

[9] E.T.J. Klompen, T.A.P. Engels, L.E. Govearts, H.E.H. Meijer, *Modeling of the postyield response of glassy polymers: Influence of thermomechanical history*, Macromolecules, 38 (2005) 6997-7008.

[10] Thompson, W. (Lord Kelvin), *On the division of space with minimal partitional area*, Philos. Mag. 24 (5th Series) (1887) 503514

[11] D. Reniers, *Skeletonization and Segmentation of Binary Voxel Shapes*, Technische Universiteit Eindhoven (2009).

[12] J.A.F. Plateau, *Statique exprimentale et theorique des liquides soumis aux seules forces molculaires*, Vol. 2 Gauthier-Villars, Paris (1873)

[13] www.mathworks.nl/company/newsletters/news_notes/win02/watershed.html

[14] Q. Li, J.G. Griffiths, *Least Squares Ellipsoid Specific Fitting*, Geometric Modeling and Processing, 2004. Proceedings, pages 335340, 2004

[15] E.W.C. Coenen, V. Kouznetsova, M.G.D. Geers, *Computational homogenization for heterogeneous thin sheets*, International Journal of Numerical Methodololgy Engineering, 83 (2010) 1180-1205

[16] A.K. van der Vegt, L.E. Goveart, *Polymeren, van keten tot kunststof*, 5th edition (2003-2005) isbn 90-71301-48-6